

Equilibrium vortex configurations in ultra-rapidly rotating two-component Bose-Einstein condensates

C.-H. Hsueh¹, T.-L. Horng², S.-C. Gou³, and W. C. Wu¹
(Dated: June 18, 2022)

The equilibrium vortex formations in rotating binary Bose gases with a rotating frequency higher than the harmonic trapping frequency is investigated theoretically. We consider the system being evaporatively cooled to form condensates and a combined numerical scheme is applied to ensure the binary system being in an authentic equilibrium state. To keep the system stable against the large centrifugal force of ultrafast rotation, a quartic trapping potential is added to the existing harmonic part. Using the Thomas-Fermi approximation, a critical rotating frequency Ω_c is derived, which characterizes the structure with or without a central density hole. Vortex structures are studied in details with rotation frequency both above and below Ω_c , and with respect to the miscible, symmetrically-separated, and asymmetrically-separated phases in their non-rotating ground-state counterparts.

I. INTRODUCTION

Quantum coherence has enabled intriguing phenomenon, such as quantized vorticity, in Bose-Einstein condensates (BECs). When a trapped condensate is driven to rotate, singly quantized vortices form. In lower rotations, only one or few vortices will be present at equilibrium [1]. Faster rotation can generate more vortices which are eventually condensed into a lattice [2–5]. Vorticity in a single-component Bose condensates has indeed been observed in a variety of experiments. On the other hand, since the first experiment of two coexisting condensates of two different hyperfine states of ⁸⁷Rb [6] was realized, BEC in mixtures of trapped quantum gases provides a unique opportunity to study the miscibility of interpenetrating quantum fluid. Several theoretical articles about binary-mixture condensates have expounded that both the interspecies and intraspecies interactions play an important role in determining the density patterns and phase separation of the condensates [7–12]. In contrast to the Abrikosov vortex-lattice state of a scalar BEC, the vortex states of binary-mixture BECs have various exotic structures due to the variety of interactions [13–15].

Rotating Bose condensates are usually confined in a harmonic trap with cylindrical symmetry around the rotation axis (say, z -direction). In these typical cases, there are two limiting regimes depending on the relative size of the rotating frequency Ω_0 and the trapping frequency ω in the xy plane. When $\Omega_0 > \omega$, the system will become unstable due to a strong centrifugal force. In order to analyze the regime of ultrafast rotations with $\Omega_0 > \omega$, one approach is to add a quartic part to the harmonic potential. In this type of system, the trapping force will be always greater than the centrifugal force and consequently the regime $\Omega_0 > \omega$ can be fully explored [16–23]. The current paper attempts to study the equilibrium vortex states of ultrafast-rotating binary condensates confined in a harmonic-plus-quartic potential.

In a single-component fast-rotating condensate, when $\Omega_0 > \omega$, the system can experience an effective potential

of Mexican-hat shape. Depending on how Ω_0 is larger than ω , the system can be roughly separated into two regimes: a condensate with or without the central density hole. More exactly, it has been shown in the literature that there exist three distinct phases for the fast-rotating scalar condensate confined in a harmonic-plus-quartic potential. One is the vortex lattice without a hole (VL), the second is the vortex lattice with a hole (VLH), and the third is the giant vortex state (GV) [19, 22]. It is interesting to see how the interspecies and intraspecies interactions play the role in the binary-mixture condensates under fast rotation and in particular, how the above-mentioned phases manifest in these systems.

Due to the complexity of the interactions in the binary system, a standard imaginary-time propagating method may not be easy to find the converging results for the true equilibrium states. It has been shown in Ref. [24] that Gross-Pitaevskii equation (GPE) with a phenomenological damping term can provide an efficient numerical machinery for finding the eigenstates of the time-independent GPE. This, a **similar** stochastic Gross-Pitaevskii equation (SGPE) approach [25–29], has been demonstrated to be an efficient way for studying the single-component BEC system. It is also anticipated that SGPE is an alternatively efficient method for studying the dynamic and equilibrium properties of a multi-component system near absolute zero.

The paper is organized as follows. In Sec. II, we introduce the theory for studying the equilibrium vortex states of a binary-mixture BEC system. To investigate the regime of ultrafast rotation, the system is trapped under a harmonic-plus-quartic potential. Sec. III is devoted to a detailed discussion of the vortex structures for fast-rotating binary-mixture BECs. A critical rotation frequency Ω_c is derived and both $\Omega < \Omega_c$ and $\Omega > \Omega_c$ regimes are studied. It will be shown explicitly that vortex structures of the system do manifest the ground states of their non-rotating counterparts. Sec. IV is a brief conclusion.

II. METHODOLOGY

We consider rapidly rotating two-component pancake-shape BECs that are parallel to the xy -plane and in a cylindrically symmetric potential. Assuming that the excitation in the z -direction is suppressed, the system can be treated approximately by a two-dimensional theory. In the mean-field approximation, such a two-component BEC system in a co-rotating frame with a rotating frequency Ω_0 around the z -axis can be described by the time-dependent coupled GPEs:

$$i\hbar \frac{\partial \Psi_j}{\partial t} = \left(\mathcal{L}_{\text{GP}}^{(j)} - \mu_j \right) \Psi_j = \left(\mathcal{H}_j + \sum_{k=1,2} U_{jk} |\Psi_k|^2 - \mu_j \right) \Psi_j, \quad (1)$$

where for component j ($= 1, 2$), $\mathcal{L}_{\text{GP}}^{(j)}$ is the GP Hamiltonian, μ_j is the chemical potential, and Ψ_j is the macroscopic wave function normalized under $N_j = \int |\Psi_j|^2 dx dy$ with N_j the particle number. $\mathcal{H}_j \equiv -\hbar^2 \nabla^2 / (2m_j) + V_j - \Omega_0 L_z$ is the single-particle Hamiltonian with m_j the atomic mass, $V_j = m_j \omega_j^2 r^2 / 2 + u_j r^4 / 4$ the trapping potential in **polar** coordinates (r, ϕ) , ω_j the harmonic trapping frequency, u_j the strength of the quartic potential, and $L_z = -i\hbar \partial / \partial \phi$ the z -component angular momentum operator. The interaction parameter $U_{jk} = 2\pi \hbar^2 \tilde{a}_{jk} (m_j^{-1} + m_k^{-1})$ with $\tilde{a}_{jk} (> 0)$ the effective two-dimensional s -wave scattering length between atoms in components j and k .

As mentioned before, it has been shown that GPE with a phenomenological damping term [24] and SGPE may be an efficient numerical approach to obtain accurate ground states of a given time-independent GPE. Here we shall apply a similar SGPE approach to study the vortex states of a ultrafast-rotating two-component BEC system. The coupled SGPEs for the present binary system can be expressed as

$$i\hbar \frac{\partial \Psi_j}{\partial t} = (1 - i\gamma) \left(\mathcal{L}_{\text{GP}}^{(j)} - \mu_j \right) \Psi_j + \eta_\gamma, \quad (2)$$

where $\eta_\gamma = \eta_\gamma(\mathbf{r}, t)$ is a complex Gaussian noise considered arising due to the contact with the thermal modes. The correlation function associated with the noise is given by $\langle \eta_\gamma^*(\mathbf{r}, t) \eta_\gamma(\mathbf{r}', t') \rangle = 2\hbar k_B T \gamma \delta(\mathbf{r} - \mathbf{r}') \delta(t - t')$. The strength of the noise, and hence the damping, is thus proportional to γ . In principle, γ can be calculated *ab initio* in terms of the Keldysh self-energy [25, 26]. However, as we are interested only in the properties at equilibrium, we may approximate it as a spatial and temporal constant. Throughout this paper, γ is reasonably taken to be a small number, 0.01. The temperature is set to be 1nK which is about 10^{-2} or less of the critical temperature of a typical BEC system. Here we have to state that the coupled SGPEs (2) do not describe the dynamics of a two-component system accurately since any coupling

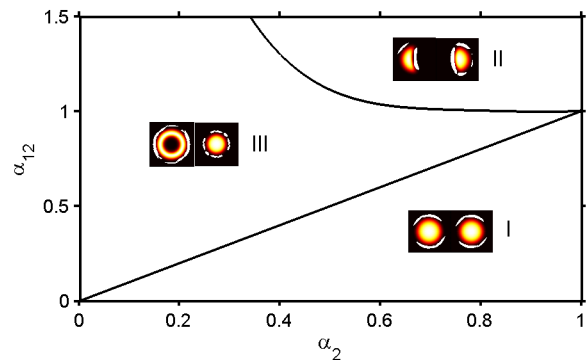


FIG. 1. Phase diagram of the non-rotating binary-mixture condensates confined in a harmonic-plus-quartic trap in terms of the relative interaction strengths, $\alpha_2 \equiv \tilde{a}_{22}/\tilde{a}_{11}$ and $\alpha_{12} \equiv \tilde{a}_{12}/\tilde{a}_{11}$. The quartic trap strength is fixed at $\lambda = 1$. Regions I, II, and III correspond to miscible, asymmetrically separated, and symmetrically separated phases, respectively.

of the thermal cloud components of the two different condensates is not considered. Because we focus on the equilibrium states, the effect of these couplings should be slight, and Eq. (2) is good enough for obtaining the equilibrium states of a two-component system.

To reduce the number of parameters, we shall assume that $m_1 = m_2 \equiv m$, $\omega_1 = \omega_2 \equiv \omega$, $u_1 = u_2 \equiv u$, and $N_1 = N_2 \equiv N$, respectively. Moreover, for convenience, the computations will be carried in the oscillator units. That is, the length, time, and energy are scaled respectively in units of $\sqrt{\hbar/m\omega}$, $1/\omega$, and $\hbar\omega$. As a consequence, the coupled SGPEs (2) take the following dimensionless forms:

$$i \frac{\partial \psi_j}{\partial t} = (1 - i\gamma) \times \left(-\frac{\nabla^2}{2} + \frac{r^2}{2} + \frac{\lambda r^4}{4} + i\Omega \frac{\partial}{\partial \phi} + \sum_{k=1,2} g_{jk} |\psi_k|^2 - \tilde{\mu}_j \right) \psi_j + \tilde{\eta}_\gamma. \quad (3)$$

Here we have redefined the normalized wave function $\psi_j \equiv \sqrt{\hbar/(m\omega N)} \Psi_j$, the strength of the quartic trap $\lambda \equiv u\hbar/(m^2\omega^3)$, the interaction constants between atoms $g_{jk} \equiv 4\pi N \tilde{a}_{jk}$, the chemical potential $\tilde{\mu}_j \equiv \mu_j/\hbar\omega$, and the noise $\tilde{\eta}_\gamma \equiv \eta_\gamma/\hbar\omega$. Besides the rotation rate $\Omega \equiv \Omega_0/\omega$. The rotation rate and the quartic trap strength will be fixed at $\Omega = 2.5$ and $\lambda = 1$ in our calculation throughout this paper.

In our calculations, the equilibrium solutions and the corresponding chemical potentials are obtained by solving the norm-preserving imaginary-time propagation of the time-dependent coupled GPEs (1) starting from an arbitrary trial wave function. The propagation continues until the fluctuation in the norm of the wave function becomes smaller than 10^{-5} . To determine whether the vortex states obtained are indeed at equilibrium, the solutions of the GPEs, which were converged by the

imaginary-time method, are then substituted into and treated as the initial states of the coupled SGPEs (2). If the initial state was not an equilibrium state, it would keep propagating until the damping term vanishing.

Moreover, we have used the method of lines with spatial discretization by the Fourier pseudospectral method to compute Eqs. (1) and (2) [or (3)]. The time integration in Eq. (1) is done by the adaptive Runge-Kutta method of order 2 and 3 (RK23), which is more time efficient due to an adjustable time step. However, the fourth-order Runge-Kutta method (RK4) is used for Eq. (2) [or (3)], since the thermal noise term η_γ is proportional to $1/\sqrt{dt}$, and is better computed with a fixed time step.

III. RESULTS AND DISCUSSIONS

A. Non-rotating ground states

Solving the non-rotating ($\Omega = 0$) time-dependent coupled GPEs (1) using the imaginary-time propagating method, we have obtained three distinct phases for the ground states of the binary-mixture condensates. Fig. 1 shows the phase diagram of the binary-mixture condensates in terms of the relative interaction strengths, $\alpha_2 \equiv \tilde{a}_{22}/\tilde{a}_{11}$ and $\alpha_{12} \equiv \tilde{a}_{12}/\tilde{a}_{11}$. By symmetry, it is sufficient to consider $\alpha_2 \leq 1$ only. The non-rotating binary-mixture condensates are phase miscible in region I and phase separated in regions II (asymmetric) and III (symmetric). As shown in Fig. 1, the boundary between phases I and III is linear, $\alpha_{12} = \alpha_2$, which is obtained by jointing nine points: from $\alpha_2 = 0.2$ to $\alpha_2 = 1$ spaced by 0.1, and their corresponding α_{12} are determined numerically with precision less than 0.01. The quartic trap (λ) has only a minimal effect on the boundary between the miscible and the symmetric separated phases. On the contrary, the boundary between phases II and III is quite λ -dependent, which is obtained by jointing nine points: from $\alpha_2 = 0.4$ to $\alpha_2 = 1$ spaced by 0.1, and their corresponding α_{12} are determined numerically with precision less than 0.01. Due to a relatively stronger confinement, the area of phase II can expand as λ increases. This allows a larger space for studying the asymmetric phase-separated regime for fast-rotating binary-mixture condensates. The two boundaries intersect at $(\alpha_2, \alpha_{12}) = (1, 1)$ which is called the *isotropic* point. We shall study the vortex structures in all three phases and in particular at the isotropic point.

B. Vortex states

Before discussing the fast-rotating binary-mixture condensates, it is useful to first examine the case of a scalar rotating condensate trapped in a harmonic-plus-quartic potential. In the one-component system, there is only one interaction constant $g \equiv 4\pi N\tilde{a}$, and when $g \gg 1$ the system is in the so-called Thomas-Fermi (TF) regime.

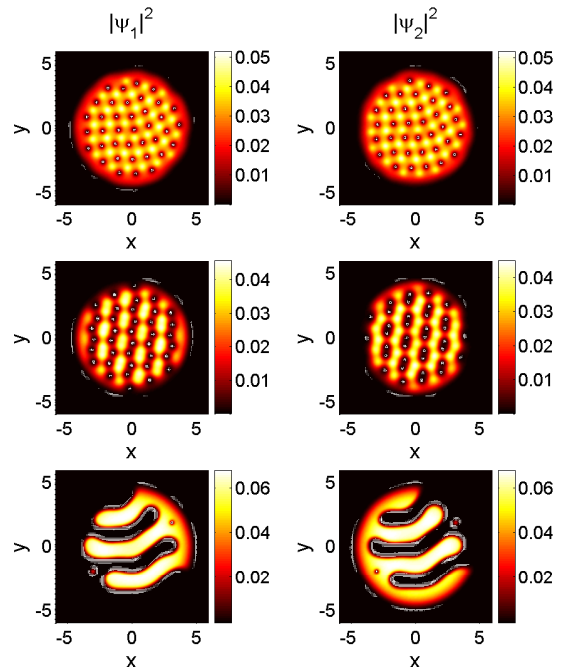


FIG. 2. (Color online) Vortex structures of individual component in fast-rotating binary-mixture condensates confined in a harmonic-plus-quartic potential. The interaction constants $g_{11} = g_{22} = 1300$ ($\alpha_2 = 1$), the rotation rate $\Omega = 2.5$, and the quartic trap strength $\lambda = 1$ for all frames. From the top to the bottom rows, $\alpha_{12} = 0.7, 1,$ and 1.3 , respectively.

The TF density can be obtained by ignoring the kinetic energy:

$$n_{\text{TF}} \equiv |\psi_{\text{TF}}|^2 = \left[\mu_{\text{TF}} + \frac{(\Omega^2 - 1)r^2}{2} - \frac{\lambda r^4}{4} \right] / g. \quad (4)$$

For $\Omega < 1$, the density has a local maximum near the center, but it changes to a local minimum for $\Omega > 1$. Eq. (4) has solutions where the TF density vanishes

$$R_{\gtrless}^2 = \frac{(\Omega^2 - 1) \pm \sqrt{4\lambda\mu_{\text{TF}} + (\Omega^2 - 1)^2}}{\lambda}. \quad (5)$$

Here the upper (plus) sign denotes the outer radius $R_{>}$ for any value of the chemical potential μ_{TF} . In contrast, the lower (minus) sign yields a physical inner radius $R_{<}$ only if μ_{TF} is negative. Correspondingly the negative chemical potential can be fixed by $\mu_{\text{TF}} = (3g\sqrt{\lambda}/\pi)^{2/3}/4 - (\Omega^2 - 1)^2/(4\lambda)$ and the spatial extension of the atomic cloud can be characterized by $R_{>}$ and $R_{<}$ which correspond to the outer and inner TF radii, respectively. Accordingly, the system can be separated into two regimes demarcated by a critical rotating frequency Ω_c corresponding to $R_{<}(\Omega_c) = 0$ [or $\mu_{\text{TF}}(\Omega_c) = 0$]. It is found that $\Omega_c^2 = 1 + (3\lambda^2 g/\pi)^{1/3}$ which is dependent of the interaction constant g and the quartic trap strength λ . At sufficiently high rotating frequencies such that $\Omega > \Omega_c$ and hence $R_{<} > 0$, a central hole will appear in the condensates, i.e., in the VLH state

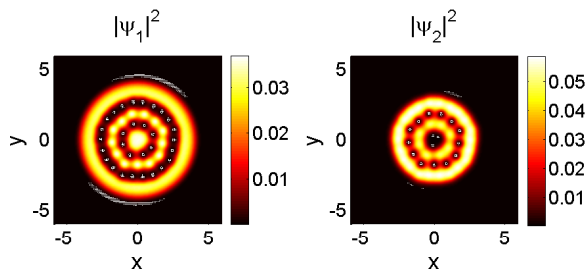


FIG. 3. (Color online) Vortex structures of component 1 (left panel) and 2 (right panel) in fast-rotating binary-mixture condensates. Here $g_{11} = 1300$, $\alpha_2 = 0.5$, $\alpha_{12} = 0.8$, $\lambda = 1$, and $\Omega = 2.5$.

[19, 22]. In contrast for $\Omega < \Omega_c$, vortex lattice without a central hole regime (the VL state) will appear.

For the present binary-mixture condensates, the critical rotating frequency Ω_c which characterizes the transition between the VL and the VLH states, can be qualitatively determined by the larger of g_{11} and g_{22} . As mentioned before, in this paper we consider only the cases $g_{11} \geq g_{22}$ (i.e., $\alpha_2 \leq 1$). Consequently

$$\Omega_c^2 \equiv 1 + (3\lambda^2 g_{11}/\pi)^{\frac{1}{3}}. \quad (6)$$

When $\Omega < \Omega_c$, the rotating binary system will be in the VL state, while when $\Omega > \Omega_c$, the system will be in the VLH state. In the following two subsections, two distinct cases of $g_{11} = 1300$ and $g_{11} = 55$ will be studied. The former corresponds to a critical rotating frequency $\Omega_c = 3.43$ and hence $\Omega = 2.5 < \Omega_c$, while the latter corresponds to $\Omega_c = 2.18$ and hence $\Omega > \Omega_c$. In the following calculations, the equilibrium vortex solutions and the corresponding chemical potentials are obtained by solving the norm-preserving imaginary-time propagation of the time-dependent coupled GPEs (1) starting from an arbitrary trial wave function. To determine whether the vortex states obtained are indeed at equilibrium, the solutions of the GPEs, which were converged by the imaginary-time method, are then substituted into and treated as the initial states of the coupled SGPEs (2).

1. VL state with $\Omega < \Omega_c$

We first consider the vortex structures with rotation frequency below the critical rotating frequency, $\Omega < \Omega_c$. Fig. 2 shows the equilibrium vortex structures of two-component condensates confined in a harmonic-plus-quartic potential with $g_{11} = g_{22} = 1300$ ($\alpha_2 = 1$) and $\alpha_{12} = 0.5, 1$, and 1.3 (from the top to the bottom) respectively. All three cases are belonging to the VL regime to which one is able to conclude for the following. (i) For a phase-miscible mixture, the equilibrium state is composed of regular vortex lattices which form roughly a square lattice at $\alpha_{12} = 0.5$ than what is expected to be a triangular lattice when $\alpha_{12} \rightarrow 0$ [30]. (ii) At the isotropic

point ($\alpha_2 = \alpha_{12} = 1$), a honeycomb lattice is formed for one component, while vortices in the other component form a vortex-pair lattice (vortex of every pair has the same circulation). (iii) Stationary vortex sheets are formed for an asymmetric phase-separated mixture. Our results in Fig. 2 are intended to be compared to those shown in Figs. 2(a), 3, and 4 in Ref. [14]. With our results, we have been able to verify that the one shown in Fig. 3(b) of Ref. [14] corresponds to an authentic equilibrium state, while the one shown in Fig. 3(a) of Ref. [14] corresponds to a transition state.

Fig. 3 shows the vortex structures of the mixtures with $g_{11} = 1300$, $\alpha_2 = 0.5$, and $\alpha_{12} = 0.8$. For these parameters, the system is still in the VL regime with $\Omega < \Omega_c$. In this case, the system has a ball-and-shell non-rotating ground state (phase III) and in the vortex state it forms an interlocking oniony vortex-sheet structure.

2. VLH state with $\Omega > \Omega_c$

The results in the VLH regime with $\Omega > \Omega_c$ are considered next. In this subsection, to see more clearly the vortex physics, we show both results of both density profile $n_j(x, y) = |\psi_j(x, y)|^2$ and phase profile given by

$$S_j(x, y) = \arctan \left[\frac{\text{Im}\psi_j(x, y)}{\text{Re}\psi_j(x, y)} \right]. \quad (7)$$

In the phase profile, the end point of the boundary between a π phase line and a $-\pi$ phase line will correspond to a vortex. In addition, the circulation and the number of vortices can also be counted directly. Fig. 4 shows the vortex structure and the corresponding phase profile of fast-rotating binary-mixture condensates with $g_{11} = 55$,

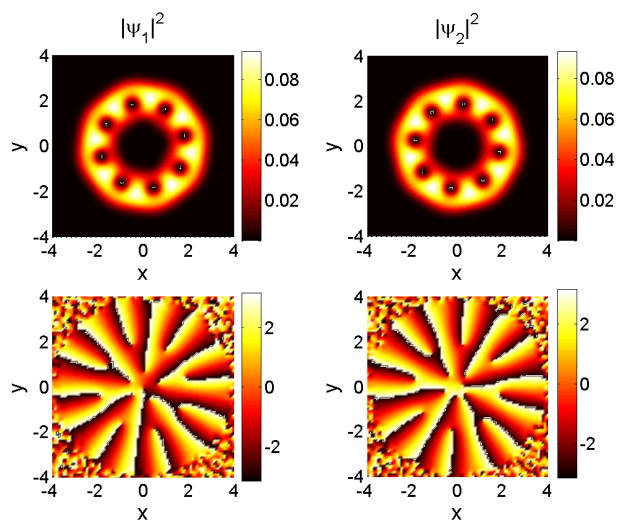


FIG. 4. (Color online) Vortex structures (top row) and phase profiles (bottom row) of component 1 (left column) and 2 (right column) of fast-rotating binary-mixture condensates. Here $g_{11} = 55$, $\alpha_2 = 1$, $\alpha_{12} = 0.5$, $\lambda = 1$, and $\Omega = 2.5$.

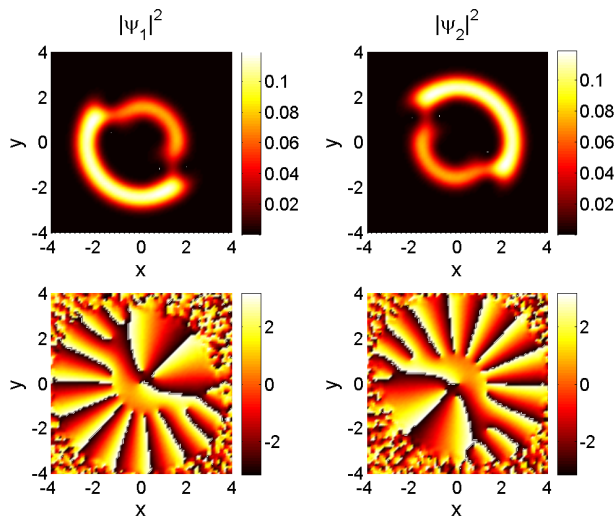


FIG. 5. (Color online) Vortex structures (top row) and phase profiles (bottom row) of component 1 (left column) and 2 (right column) of fast-rotating binary-mixture condensates. Here $g_{11} = 55$, $\alpha_2 = 1$, $\alpha_{12} = 1.3$, $\lambda = 1$, and $\Omega = 2.5$.

$\alpha_2 = 1$, and $\alpha_{12} = 0.5$. The ground state of the corresponding non-rotating condensate mixture is miscible (phase I) to which the wavefunctions of the two components overlap entirely. In view of Fig. 4, it is found that the two annular vortex arrays are interlocking in a manner that density peak of one component is located at the density hole of the other component.

Fig. 5 shows the vortex structure and the corresponding phase profile of the mixture with $g_{11} = 55$, $\alpha_2 = 1$, and $\alpha_{12} = 1.3$. The non-rotating counterpart has an asymmetric separated ground state (phase II in Fig. 1). Due to the strong repulsive interaction between two condensates which results the asymmetric separated characteristic, the two condensates occupy on the opposite side of each other.

Fig. 6 shows the vortex structure and the corresponding phase profile of a condensate mixture with $g_{11} = 55$, $\alpha_2 = 0.5$, $\alpha_{12} = 0.8$. With respect to phase III in Fig. 1, the non-rotating mixture has a ball-and-shell ground state, *i.e.*, the component with larger intraspecies interaction occupying the outside and forming a shell, while the component with smaller intraspecies interaction occupying the inside and forming a ball. It is found that vortices in component 1 (of larger intraspecies interaction) form a circular array around the central low-density hole, while vortices in component 2 (of smaller intraspecies interaction) also form a circular array which is closer to the center (see the inset of the density profile or the phase profile plot). In addition to the vortices, the “ball” of the non-rotating counterpart of component 2 is actually pushed away (due to fast rotation) from the center and forms a robust ringlike condensate located at where the vortices of component 1 are (*i.e.*, interlocking). This robustness actually resists its own vortices revolving into it.

In Fig. 7, we have also shown the vortex structure

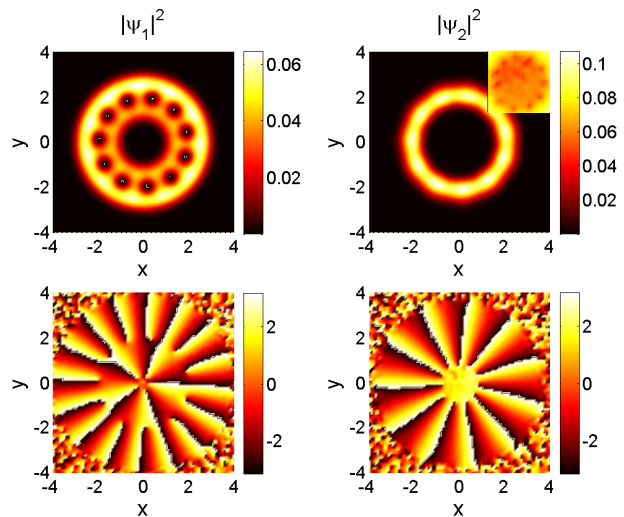


FIG. 6. (Color online) Vortex structures (top row) and phase profiles (bottom row) of component 1 (left column) and 2 (right column) of fast-rotating binary-mixture condensates. Here $g_{11} = 55$, $\alpha_2 = 0.5$, $\alpha_{12} = 0.8$, $\lambda = 1$, and $\Omega = 2.5$. The inset shows a more clear view of the vortices in component 2.

and its corresponding phase profile of a mixture at the isotropic point, with $g_{11} = 55$, $\alpha_2 = \alpha_{12} = 1$. Similar to the result of the middle row of Fig. 2, fast-rotating condensates tend to form the vortex-pair structure at the isotropic point.

C. Concluding Remarks

The overall features of vortex structures in ultrafast-rotating binary-mixture condensates can be understood as follows. Pertaining to phase I in Fig. 1, when $\alpha_{12} = 0$ where the two components are not interacting with each other, the theory is essentially reduced to the one for single components. In this limit, triangular vortex lattices are expected to form with $\Omega < \Omega_c$, while annular vortex arrays are expected to form with $\Omega > \Omega_c$. As α_{12} is present and increases, vortex cores of one component gradually shift away from those of the other component and consequently with $\Omega < \Omega_c$ the triangular lattices are distorted. Eventually the vortices for each component will form a square lattice instead of a triangular one. As α_{12} exceeds α_2 , equivalently for the system to shift to phase II or III, the condensates can undergo phase separation to spontaneously form domains. For one condensate, the cavity of another condensate is where the lower effective potential is, which is more apt to be occupied. However, more interlocking will cause wavefunctions overlap more and at the same time raise the interspecies interaction energy $\propto g_{12} |\Psi_1|^2 |\Psi_2|^2$. In order to prevent the above-mentioned interlocking that causes high energies, the vortices are actually concentrated out of the condensates and form the vortex sheets. Consequently the two components form comple-

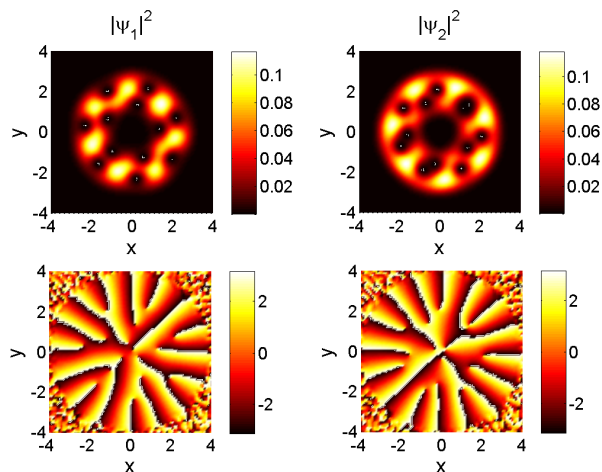


FIG. 7. (Color online) Vortex structures (top row) and phase profiles (bottom row) of component 1 (left column) and 2 (right column) of fast-rotating binary-mixture condensates. Here $g_{11} = 55$, $\alpha_2 = 1$, $\alpha_{12} = 1$, $\lambda = 1$, and $\Omega = 2.5$.

mentary structures to each other and the total density will be roughly described by the Thomas-Fermi distribution $|\Psi_1|^2 + |\Psi_2|^2 \propto \max[\mu_{\text{TF}} - (m\omega^2 r^2/2 + ur^4/4), 0]$. The results in the bottom row of Fig. 2 as well as in Figs. 3, 5, and 6 are examples of this kind.

IV. CONCLUSION

This paper investigates the equilibrium vortex structures of ultrafast-rotating binary-mixture condensates

trapped in a harmonic-plus-quartic potential. In contrast to the harmonic trap alone case where the system is unstable when the rotation alone frequency Ω_0 is higher than the radial trap oscillator frequency ω , the added quartic trap can lead the system to remain stable at higher rotation velocity ($\Omega_0 > \omega$). Due to the complexity of interactions in the binary system, there often occur many metastable states in the fast-rotating two-component condensate system and the standard imaginary-time propagating approach may not really converge to the true equilibrium states of the system. In this regard, we have applied a combined numerical scheme to effectively assure that the density profiles do really saturate at sufficiently low temperatures. A critical rotating frequency Ω_c which characterizes the transition between the VL and the VLH states is identified. Under high rotation frequencies ($\Omega_0 > \omega$), a variety of vortex structures of the two-component condensates are shown for $\Omega < \Omega_c$, similar to those presented in Ref. [14], and also for $\Omega > \Omega_c$ in particular to which various annular vortex structures occur.

V. ACKNOWLEDGMENTS

This work was supported by National Science Council of Taiwan (Grant Nos. 99-2112-M-003-006-MY3 and 98-2112-M-018-001-MY2). We also acknowledge the support from the National Center for Theoretical Sciences, Taiwan.

-
- [1] M. R. Matthews, B. P. Anderson, P. C. Haljan, D. S. Hall, C. E. Wieman, and E. A. Cornell, Phys. Rev. Lett. **83**, 2498 (1999).
 - [2] J. R. Abo-Shaeer, C. Raman, J. M. Vogels, and W. Ketterle, Science **292**, 476 (2001).
 - [3] C. Raman, J. R. Abo-Shaeer, J. M. Vogels, K. Xu, and W. Ketterle, Phys. Rev. Lett. **87**, 210402 (2001).
 - [4] P. C. Haljan, I. Coddington, P. Engles, and E. A. Cornell, Phys. Rev. Lett. **87**, 210403 (2001).
 - [5] P. Engles, I. Coddington, P. C. Haljan, and E. A. Cornell, Phys. Rev. Lett. **89**, 100403 (2002).
 - [6] C. J. Myatt, E. A. Burt, R. W. Ghrist, E. A. Cornell, and C. E. Wieman, Phys. Rev. Lett. **78**, 586 (1997).
 - [7] B. D. Esry, and C. H. Greene, Phys. Rev. A **59**, 1457 (1999).
 - [8] M. Trippenbach, K. Góral, K. Rzążewski, B. Malomed, and Y B Band, J. Phys. B **33**, 4017 (2000).
 - [9] F. Riboli, and M. Modugno, Phys. Rev. A **65**, 063614 (2002).
 - [10] D. M. Jezek, and P. Capuzzi, Phys. Rev. A **66**, 015602 (2002).
 - [11] A. A. Svidzinsky, and S. T. Chui, Phys. Rev. A **67**, 053608 (2003).
 - [12] C. C. Huang, and W. C. Wu, Phys. Rev. A **75**, 023609 (2007).
 - [13] E. J. Mueller and T. L. Ho, Phys. Rev. Lett. **88**, 180403 (2002).
 - [14] K. Kasamatsu, M. Tsubota, and M. Ueda, Phys. Rev. Lett. **91**, 150406 (2003).
 - [15] S. J. Woo, S. Choi, L. O. Baksmaty, and N. P. Bigelow, Phys. Rev. A **75**, 031604(R) (2007).
 - [16] E. Lundh, Phys. Rev. A, **65**, 043604 (2002).
 - [17] K. Kasamatsu, M. Tsubota, and M. Usda, Phys. Rev. A **66**, 053606 (2002).
 - [18] P. Engels, I. Coddington, P. C. Haljan, V. Schweikhard, and E. A. Cornell, Phys. Rev. Lett. **90**, 170405 (2003).
 - [19] G. M. Kavoulakis and G. Baym, New J. Phys. **5**, 51 (2003).
 - [20] V. Bretin, S. Stock, Y. Seurin, and J. Dalibard, Phys. Rev. Lett. **92**, 050403 (2004).
 - [21] T. P. Simula, A. A. Penckwitt, and R. J. Ballagh, Phys. Rev. Lett. **92**, 060401 (2004).
 - [22] A. L. Fetter, B. Jackson, and S. Stringari, Phys. Rev. A **71**, 013605 (2005).
 - [23] C. C. Huang, C. H. Liu, and W. C. Wu, Phys. Rev. A **81**, 043605 (2010).

- [24] S. Choi, S. A. Morgan, and K. Burnett, Phys. Rev. A **57**, 4057 (1997).
- [25] H. T. C. Stoof, J. Low Temp. Phys. **114**, 11 (1999).
- [26] H. T. C. Stoof, J. Low Temp. Phys. **124**, 431 (2001).
- [27] C. W. Gardiner, J. R. Anglin, and T. I. A. Fudge, J. Phys. B **35**, 1555 (2002).
- [28] C. W. Gardiner and M. J. Davis, J. Phys. B **36**, 4731 (2003).
- [29] A. S. Bradley, C. W. Gardiner, and M. J. Davis, Phys. Rev. A **77**, 033616 (2008).
- [30] As discussed in Ref. [14], interaction energy E_{int} can be expressed in term of the total density $n = |\Psi_1|^2 + |\Psi_2|^2$ and the spin variable $S = |\Psi_1|^2 - |\Psi_2|^2$ as $E_{int} = (C_{11}/8) \int d\mathbf{r} [(1 + \alpha_2 + 2\alpha_{12})n^2 + (1 + \alpha_2 - 2\alpha_{12})S^2 + 2(1 - \alpha_2)nS]$. If the coefficient $(1 + \alpha_2 - 2\alpha_{12})$ is positive, antiferromagnetism manifests and makes a square lattice stabilized.